



# In vitro and in vivo characterization of antibacterial activity and biocompatibility: A study on silver-containing phosphonate monolayers on titanium



Carmen-Mihaela Tîlmaciu<sup>a,1</sup>, Marc Mathieu<sup>b,c,1</sup>, Jean-Philippe Lavigne<sup>d</sup>, Karine Toupet<sup>b</sup>, Gilles Guerrero<sup>a</sup>, Arnaud Ponche<sup>e</sup>, Julien Amalric<sup>f</sup>, Danièle Noël<sup>b,c,\*,2</sup>, P. Hubert Mutin<sup>a,\*,2</sup>

<sup>a</sup> Institut Charles Gerhardt Montpellier, UMR 5253 CNRS-UM2-UM1-ENSCM, Université de Montpellier 2, 34095 Montpellier, France

<sup>b</sup> Inserm U844, Hôpital Saint-Eloi, Montpellier F-34295, France

<sup>c</sup> Université Montpellier1, UFR de Médecine, Montpellier F-34967, France

<sup>d</sup> Inserm U1047, Université Montpellier 1, UFR de Médecine, Nîmes, France

<sup>e</sup> Institut de Science des Matériaux de Mulhouse, UMR 7361 CNRS, 68057 Mulhouse Cedex, France

<sup>f</sup> Science et Surface, Centre Scientifique Auguste Moiroux, 64 chemin des Mouilles, 69134 Ecully Cedex, France

## ARTICLE INFO

### Article history:

Received 22 July 2014

Received in revised form 18 December 2014

Accepted 23 December 2014

Available online 3 January 2015

### Keywords:

Monolayer

Biofilm

Antibacterial

Cytotoxicity

Biocompatibility

## ABSTRACT

Infections associated with implanted medical devices are a major cause of nosocomial infections, with serious medical and economic repercussions. A variety of silver-containing coatings have been proposed to decrease the risk of infection by hindering bacterial adhesion and biofilm formation. However, the therapeutic range of silver is relatively narrow and it is important to minimize the amount of silver in the coatings, in order to keep sufficient antibacterial activity without inducing cytotoxicity. In this study, the antibacterial efficiency and biocompatibility of nanocoatings with minimal silver loading ( $\sim 0.65 \text{ nmol cm}^{-2}$ ) was evaluated in vitro and in vivo. Titanium substrates were coated by grafting mercaptododecylphosphonic acid (MDPA) monolayers followed by post-reaction with  $\text{AgNO}_3$ . The MDPA/ $\text{AgNO}_3$  nanocoatings significantly inhibited *Escherichia coli* and *Staphylococcus epidermidis* adhesion and biofilm formation in vitro, while allowing attachment and proliferation of MC3T3-E1 preosteoblasts. Moreover, osteogenic differentiation of MC3T3 cells and murine mesenchymal stem cells was not affected by the nanocoatings. Sterilization by ethylene oxide did not alter the antibacterial activity and biocompatibility of the nanocoatings. After subcutaneous implantation of the materials in mice, we demonstrated that MDPA/ $\text{AgNO}_3$  nanocoatings exhibit significant antibacterial activity and excellent biocompatibility, both in vitro and in vivo, after postoperative seeding with *S. epidermidis*. These results confirm the interest of coating strategies involving subnanomolar amounts of silver exposed at the extreme surface for preventing bacterial adhesion and biofilm formation on metallic or ceramic medical devices without compromising their biocompatibility.

© 2014 Acta Materialia Inc. Published by Elsevier Ltd. All rights reserved.

## 1. Introduction

Infections associated with the insertion or implantation of medical devices (e.g. catheters, stents, fracture fixation devices, dental implants, joint prostheses or cardiac pacemakers) are a major

\* Corresponding authors at: Inserm U844, Hôpital Saint-Eloi, Montpellier F-34295, France. Tel.: +33 4 9963 6026; fax: +33 4 9963 6020 (D. Noël), Institut Charles Gerhardt Montpellier, UMR 5253, Université de Montpellier 2, 34095 Montpellier, France. Tel./fax: +33 4 6714 4943 (P.H. Mutin).

E-mail addresses: [daniele.noel@inserm.fr](mailto:daniele.noel@inserm.fr) (D. Noël), [hubert.mutin@univ-montp2.fr](mailto:hubert.mutin@univ-montp2.fr) (P.H. Mutin).

<sup>1,2</sup> Both authors contributed equally to this work.

cause of nosocomial infections, with serious medical consequences and huge socioeconomic repercussions [1–3]. Device-related infections are usually due to colonization by opportunistic bacteria that, taking advantage of the decreased body defenses, are able to irreversibly attach and grow on the biomaterial surface, eventually forming bacterial biofilms. Bacterial biofilms can be defined as “structured communities of bacterial cells enclosed in a self-produced polymeric matrix” [4], and they have been found on most indwelling medical devices [4,5]. Bacteria in biofilms exhibit a dramatically increased resistance to host defenses or antibiotic treatments [2,3,6], which makes the treatment of biofilm infections on implants very difficult, requiring in most cases the removal of the contaminated device.

Therefore, it is crucial to prevent bacterial biofilm formation, and much attention has been devoted to the design of biomaterials with infection-resistant surfaces. Rather than developing new types of biomaterials, the most commonly used approach is based on the surface modification of existing biomaterials by a coating, which can be either passive (antifouling coating able to hinder bacterial adhesion) or active (bactericidal coating, able to kill bacteria on contact before the establishment of the biofilm). Various types of antibacterial coatings have been proposed, including polymers, hydrogels, polyelectrolyte multilayers, self-assembled monolayers, grafted antimicrobial peptides or antibiotics, calcium phosphate or sol-gel coatings, and grafted metallic nanoparticles. Several articles reviewing this field have recently been published [7–12].

Among the different types of coatings that can be used to prevent biofilm formation on inorganic substrates, self-assembled monolayers (SAMs), or more generally organic monolayers, obtained by chemisorption of organic molecules present interesting features. SAMs are nanometric coatings, with thicknesses in the 1–3 nm range depending on the size of the chemisorbed molecules. Although the majority of studies concerns model substrates such as gold or oxidized silicon surfaces, SAMs can be formed on all inorganic biomaterials (metals, ceramics or glasses) by choosing the appropriate head function (e.g. thiol, trialkoxysilane, carboxylic or phosphonic acid) [13–16]. The terminal groups in SAMs are located at the extreme surface, allowing precise control of surface properties with a minimal amount of organic molecule ( $<1 \text{ nmol cm}^{-2}$ ), simply by varying the nature and repartition of these end-groups.

Most examples of antibacterial monolayers concern passive SAMs terminated by hydrophilic groups such as oligoethylene glycol or zwitterionic groups [17–24]. There are also several examples of active bactericidal SAMs, which are based either on terminal cationic groups [20,25,26] or on terminal complexing groups such as carboxylate, thiol or bipyridine groups, able to bind antimicrobial metal ions such as silver or copper ions [22,27–29]. Additionally, SAMs or more generally functional monolayers have been used as intermediate layers for, among other things, the anchoring of antibiotics [30] antimicrobial peptides [31] or silver nanoparticles [32,33].

Silver ions ( $\text{Ag}^+$ ) are a well-known broad-spectrum bactericide exhibiting bactericidal or bacteriostatic activity at very low concentrations [34]. Coatings containing  $\text{Ag}^+$  or silver nanoparticles (acting as a reservoir of  $\text{Ag}^+$ ) are increasingly used in medical devices such as wound dressings and catheters and their antibacterial activity is well established [11,35]. It is usually assumed that the toxicity of  $\text{Ag}^+$  against human cells is lower than against bacteria. However, recent studies suggest that the toxic effect of  $\text{Ag}^+$  toward bacteria and human cells occurs in the same concentration range [35,36]. It is thus important to minimize the amount of silver in the coatings, in order to keep sufficient antibacterial activity without inducing cytotoxicity [37,38].

In a previous work, we have reported the formation of antibacterial monolayers on titanium and stainless steel substrates, by surface modification with a phosphonate monolayer in two steps: (i) deposition of a thiol-terminated SAM by immersion of the substrate in a mercaptododecylphosphonic acid (MDPA) solution (grafting by formation of Ti–O–P bonds); (ii) post-modification of the thiol end-groups by silver nitrate to form silver thiolate end-groups (Fig. 1). The silver content in these SAMs is limited by the maximum density of a SAM ( $\sim 5$  phosphonate molecule  $\text{nm}^{-2}$ ) and is thus extremely low ( $<1 \text{ nmol}$  or  $0.1 \mu\text{g Ag cm}^{-2}$ ) compared to most other Ag-containing coatings reported in the literature. Despite this low Ag content, the adhesion of *Escherichia coli*, *Staphylococcus aureus*, *Staphylococcus epidermidis* and *Pseudomonas aeruginosa* to coated metal surfaces was strongly decreased and the growth of a biofilm was inhibited for several days [27],

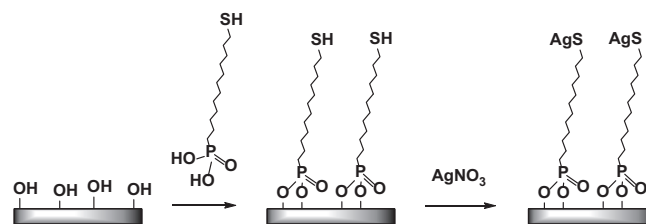


Fig. 1. Schematic illustration of the surface modification of a titanium substrate by a MDPA SAM, followed by post-reaction with  $\text{AgNO}_3$ .

demonstrating that minimal amounts of silver localized at the extreme surface could confer interesting antibacterial properties to metallic biomaterials.

In the present work we further confirmed the interest of these silver-modified SAMs as antibacterial coatings for titanium-based medical devices, by demonstrating, after sterilization by ethylene oxide (EO), their *in vitro* and *in vivo* antibacterial activity, as well as their nontoxicity *in vitro* toward osteoblasts and mesenchymal stem cells (MSCs), which are cells of the bone microenvironment, and their *in vivo* biocompatibility after subcutaneous implantation in mice.

## 2. Materials and methods

### 2.1. Ti substrates and chemical compounds

Ti substrates (99.7%, Aldrich, 0.127 mm thick) of  $18 \times 18 \text{ mm}^2$  were used for water contact angle measurements and *in vitro* bacterial adhesion and biofilm assays. The size of samples for *in vitro* cytotoxicity was  $10 \times 10 \text{ mm}^2$ . Ti discs (10 mm in diameter) were used for X-ray photoelectron spectroscopy (XPS) analysis, *in vivo* biocompatibility and antibacterial testing. Additionally, time-of-flight secondary ion mass spectrometry (ToF-SIMS) analysis and *in vitro* LIVE/DEAD tests were performed using 1 mm thick,  $10 \times 10 \text{ mm}^2$  Ti substrates (grade 2, Titane Services, France).

Pentane (VWR), absolute ethanol (VWR), HPLC-grade water (ACROS), chloroform (VWR) and silver nitrate (Sigma–Aldrich, >99.8%) were used as received for the grafting and washing procedures. MDPA was prepared according to the literature [39]. Silver nitrate ( $\text{AgNO}_3$ , Sigma–Aldrich, >99.8%) was used as received.

### 2.2. Surface modification

The Ti substrates were first washed by sonication in a pentane bath for 5 min, then dried and treated in an UV– $\text{O}_3$  reactor for 30 min per face in order to remove the physisorbed organic species. The cleaned substrates were modified by immersion in a degassed absolute ethanol solution of 1 mM MDPA for 48 h, in the dark and at room temperature, then rinsed with absolute ethanol, water and chloroform, and dried for 2 min under an argon flow. The resulting samples grafted by MDPA (hereinafter denoted as Ti-SH) were next immersed for 2 h in a degassed aqueous solution of 1 mM  $\text{AgNO}_3$  in the dark at room temperature, to form the silver thiolate-modified Ti substrates (hereinafter denoted as Ti-SAg), then rinsed with absolute ethanol, water and chloroform, and dried for 2 min under an argon flow. Samples were kept under argon and protected from light at  $4^\circ\text{C}$  for 1–2 months before sterilization by EO and/or use in biological assays.

### 2.3. Sterilization procedure

The Ti-SAg samples were sterilized by EO in an autoclave at  $45^\circ\text{C}$  for 3 h and packaged individually (Steriservice Bernay,

France). The sterilized non-modified and SAg-modified samples are further labeled Ti EO and Ti-SAg EO, respectively.

#### 2.4. Characterization techniques

Water contact angle measurements were performed on a GBX Digidrop Fast 60 apparatus, using 2  $\mu$ l drops of HPLC-grade water. For each type of substrate two different samples were used, and 10 measurements were performed on both faces of each sample. The values reported herein are the averages of the 40 values obtained.

XPS analysis was carried out using a Gamdata Scienta SES 2002 X-ray photoelectron spectrometer under ultra-high vacuum ( $P < 10^{-9}$  mbar). The monochromated Al  $K_{\alpha}$  source was operated at a current of 30 mA and 14 kV, with a 90° nominal take-off angle (angle between the sample surface and photoemission direction). The samples were outgassed in several ultra-high-vacuum chambers with an isolated pumping system and pressure control until transfer to the analysis chamber. Nevertheless, they were analyzed without further cleaning process and thus, the carbon contamination is still on the surface. Classical Scofield sensitivity factors were used for peak-fitting procedures with CASAXPS software (version 2.3.14; CASA Software Ltd., Devon, U.K, [www.casaxp.com](http://www.casaxp.com)): C1s 1.00, O1s 2.83, Ti2p 7.81, S2p 1.68, Ag3d 18.06 and P2p 1.19. All lineshapes used in peak fitting procedures were a mix of 30% Gaussian and 70% Lorentzian shapes.

ToF-SIMS analysis was performed by using a TOFSIMS 5 (ION-TOF GmbH, Münster, Germany), with a primary ion source of liquid Bi, an energy of 25 keV, an analysis area of  $100 \times 100 \mu\text{m}^2$  and a depth of  $< 1$  nm. A Reflectron detector for the ToF was used at a  $P < 10^{-6}$  mbar. The use of a very weak primary ion current (static SIMS) makes it possible to limit the analyzed depth (2 or 3 first atomic layers) and also to limit the fragmentation (enable surface molecular analysis). Precautions were taken during handling of the samples to prevent contamination. Hence, the samples sent for analysis were covered in aluminium foil and conditioned under argon.

#### 2.5. Cell culture

Primary MSCs were isolated from C57BL/6 mice and fully characterized previously [40]. The C3-Luc MSC clone stably expressing the firefly luciferase was derived from C3H10T1/2 murine MSCs as already described [41]. Primary and C3-Luc MSCs as well as the pre-osteoblastic cell line MC3T3-E1 were maintained in proliferative medium consisting of Dulbecco's modified Eagle's medium (DMEM) supplemented with 2 mM glutamine, 100 U  $\text{ml}^{-1}$  penicillin, 100  $\mu\text{g} \text{ml}^{-1}$  streptomycin and 10% fetal calf serum (FCS).

#### 2.6. Cell proliferation and cytotoxicity assays

MC3T3-E1 cells were seeded at  $1 \times 10^3$  cells  $\text{cm}^{-2}$  and treated with MDPA or/and  $\text{AgNO}_3$  diluted in proliferative medium. Cell number was determined with a counting analyzer (Beckman Coulter). MC3T3-E1 cells were also seeded at  $1 \times 10^3$  cells  $\text{cm}^{-2}$  on cell culture treated polystyrene plastic surface (PS), or on plates of Ti, Ti-SAg or Ti-SAg EO placed in dishes with ultra-low attachment surface. Cell counts were determined as above.

#### 2.7. Osteogenic differentiation

MC3T3-E1 and MSCs were seeded at  $3 \times 10^3$  cells  $\text{cm}^{-2}$  in proliferative medium and grown for 7 days until confluence. These were then changed to osteoinductive medium consisting of DMEM supplemented with 10% FCS, 2 mM glutamine, 100 U  $\text{ml}^{-1}$  penicillin, 100  $\mu\text{g} \text{ml}^{-1}$  streptomycin, 50  $\mu\text{g} \text{ml}^{-1}$  ascorbic acid and 3 mM sodium dihydrogen phosphate. Control cells were maintained in

proliferative medium. Medium changes were performed every 3–4 days.

At day 21 post-seeding, differentiation was evaluated by measuring the expression of osteogenic markers by real time reverse transcription polymerase chain reaction (RT-PCR). Osteogenic differentiation was further assessed by quantifying alkaline phosphatase activity and by revealing the presence of calcific deposition using Alizarin Red S staining. Alkaline phosphatase activity was measured in cell supernatants diluted 1/100 in 0.05 M pH 9.5 glycine/NaOH buffer. 100  $\mu$ l of sample was mixed with 200  $\mu$ l of *para*-nitrophenylphosphate at 1 mg  $\text{ml}^{-1}$  in glycine/NaOH buffer. After 30 min incubation at 37 °C, the optical density (OD) was read at 405 nm in a spectrophotometer. Alizarin Red S staining was carried out as follows. Cells were rinsed three times with phosphate buffered saline (PBS), fixed in 95% ethanol for 30 min, washed twice with distilled water, incubated for 5 min in a 2% pH 4.2 Alizarin Red S aqueous solution, and rinsed five times with distilled water. Snapshots were taken and samples were then treated for 15 min under agitation with 10% cetylpyridinium chloride (Sigma-Aldrich) in PBS to solubilize the dye. The OD was read at 562 nm in a spectrophotometer.

#### 2.8. Fluorescence microscopy

Cells were trypsinized and labeled using the fluorescent lipophilic cationic indocarbocyanine dye CM-Dil following the manufacturer's recommendations (Invitrogen) and plated on cell culture dishes containing or not Ti substrates. After 16 h, the red emission of adherent cells was visualized by fluorescence microscopy (Zeiss Axiovert 200 M).

#### 2.9. RNA extraction, reverse transcription and real time RT-PCR

Total RNA was isolated using RNeasy mini kit (Qiagen) and reverse-transcribed using a GeneAmp Gold RNA PCR Core kit (Applied Biosystems). Real-time RT-PCR (RT-qPCR) was performed using LightCycler 480 SYBR Green I Master mix and real-time PCR instrument (Roche). PCR conditions were 95 °C for 5 min followed by 40 cycles of 15 s at 95 °C, 10 s at 64 °C and 20 s at 72 °C. For each reaction, a single amplicon with the expected melting temperature was obtained. Primer pairs were designed using the web-based applications Primer3 and BLAST at the National Center for Biotechnology Information, and were as follows: 5'-CTGAGTCTGACAAAGCCTTC-3' and 5'-GCTGTGACATCCATACTTGC-3' for the bone gamma carboxyglutamate protein/osteocalcin (Bglap) gene, 5'-ACAGTCCCAACTTCTGTGC-3' and 5'-ACGGTAACCACAGTCC-CATC-3' for the Runt-related transcription factor 2 (Runx2) gene, and GCTGTGTGACGCTAGACGAGA-3' and 5'-ATCTTCAGGCC AGGATGTA-3' for the ribosomal protein S9 (Rps9) gene. Expression of the housekeeping gene encoding Rps9 was measured for normalization. The threshold cycle (Ct) of each amplification curve was calculated by Roche's LightCycler 480 software using the second derivative maximum method. The relative amount of a given mRNA was calculated using the  $\Delta\Delta\text{Ct}$  method.

#### 2.10. Adhesion assay

Bacterial adhesion and biofilm assays were performed using two different reference strains: *E. coli* ATCC 25922 and *S. epidermidis* ATCC 12228 purchased from AES Chemunex. The inhibition of bacterial adhesion was investigated in a static system. 300  $\mu$ l of a bacterial culture diluted to an  $\text{OD}_{600}$  of 0.5 was added into the wells of six-well culture plates containing 3 ml of Mueller–Hinton broth. The final bacterial concentration in each well was  $\sim 10^5$  colony forming units per ml (cfu  $\text{ml}^{-1}$ ). The samples were immersed in the wells and incubated for 2 h at 37 °C. Following incubation,

the samples were rinsed three times with 500  $\mu\text{l}$  of sterile saline (NaCl, 0.9% w/v) to remove non-adherent bacteria. The loosely adherent bacteria were removed by vortexing and sonication in sterile saline and the bacteria in the resulting suspensions were counted by serial dilution and plating onto Luria agar. The strongly adherent bacteria remaining on the samples were transferred by blotting each side of the samples 15 times successively onto pre-dried Luria agar plates. Colony counts were performed following an overnight incubation at 37 °C. The total population of viable adherent bacteria was obtained by adding the two values [42].

### 2.11. Biofilm assay

Bacterial biofilms were grown on the surface of the samples in a static system. Overnight cultures grown in Mueller–Hinton broth were diluted to an optical density  $\text{OD}_{600}$  of 0.5. The different samples were placed vertically in a 12-well plate containing 2 ml of Mueller–Hinton growth medium, and 200  $\mu\text{l}$  of the bacterial suspension in PBS was added. Only PBS was added to the wells containing the control samples. The plates were incubated statically for 72 h at 37 °C with 5%  $\text{CO}_2$ . Under these conditions a thick biofilm formed on the bare substrates at the air–liquid interface. The substrates were then washed three times with 500  $\mu\text{l}$  of sterile PBS to remove non-adherent bacteria. The density of biofilm was assessed using colorimetry as follows. The adherent bacteria on the samples were stained with crystal violet (0.1%, 10 min). The plate was then vigorously washed three times with water, and the crystal violet was dissolved in 300  $\mu\text{l}$  of DMSO by pipetting up and down. Absorbance was read at 600 nm using a microplate reader (Multiskan Ascent, Thermo Electron, St Herblain, France). The OD values reported were obtained by subtracting the OD measured for pure DMSO.

### 2.12. LIVE/DEAD assays

Viability of adherent bacteria was assessed using the LIVE/DEAD BacLight bacterial viability kit (Invitrogen). Bacterial suspensions ( $\text{OD}_{600} = 0.05$ ,  $\sim 1 \times 10^5$  cfu  $\text{mL}^{-1}$ ) were prepared. The Ti substrates were immersed in wells containing the bacterial suspension and incubated for 2 h at 37 °C. The samples were then rinsed three times with PBS and the remaining adherent bacteria were stained with the LIVE/DEAD reagents for 15 min at room temperature in the dark as recommended by the manufacturer. The samples were then washed three times with PBS to remove non-specific stain [30]. The live (green) and dead (red) adherent bacteria on the substrates were visualized by fluorescence microscopy.

### 2.13. Animals

For all the in vivo experiments SCID/Bg and DBA/1 mice were grown in our animal facility and cared for according to the Laboratory Animal Care Guidelines. The protocol was approved by the Committee on the Ethics of Animal Experiments in Languedoc-Roussillon (CEEA-LR 36) (Permit No. CEEA-LR-13010).

### 2.14. In vivo biocompatibility assays

Tolerance of non-modified Ti EO or functionalized Ti-SAg EO implants was evaluated in immunocompetent DBA/1 mice after subcutaneous implantation of 10 mm diameter discs in the back of anesthetized mice. Mice were killed at either day 7 or day 21 after implantation. Tissues surrounding implants were fixed in 4% formaldehyde solution for 24 h and processed for routine histology. Sections (3  $\mu\text{m}$ ) were deparaffinized and hydrated before staining with hematoxylin and eosin solution.

### 2.15. In vivo bioluminescence imaging

Ti or Ti-SAg discs were subcutaneously implanted in SCID/Bg mice. Before implantation, the discs were seeded with  $2 \times 10^6$  C3-Luc cells and incubated at 37 °C for 5 h. As control, SCID/Bg mice were subcutaneously injected with  $2 \times 10^6$  C3-Luc cells in 100  $\mu\text{l}$  of PBS. Mice were monitored using noninvasive, whole-body imaging of luciferase activity and a cooled charge-coupled device (CCD) camera (NightOWL LB Berthold Technologies). Ten minutes before analysis, mice were injected intraperitoneally with 300  $\mu\text{l}$  of luciferin (Promega, Charbonnières, France) at 10  $\text{mg mL}^{-1}$  in PBS and anesthetized. Photon emission was recorded for 10 min and signal intensities were quantified using the WinLight Software (Berthold Technologies). Background intensity was obtained from a non-luminescent area of similar size, and was subtracted from the luminescent signal intensity.

### 2.16. In vivo antibacterial activity assay

Ti EO or Ti-SAg EO implants were subcutaneously implanted in DBA1 mice. After implantation of the discs and suture of the skin,  $1 \times 10^4$  cfu of *S. epidermidis* in 50  $\mu\text{l}$  of PBS were injected onto the implants. The mice were killed at day 14. Discs were recovered, placed in 1 ml sterile PBS, vortexed and crushed with a sterile scalpel. The bacteria in the resulting suspensions were counted after serial dilutions and plating. 100  $\mu\text{l}$  of each dilution were cultured on different specific agar media (Chapman, blood agar, Drigalski) for a maximum of 7 days at 37 °C to ensure optimal growth of the colonies, then the colonies were counted.

In parallel, the discs were immersed in Mueller–Hinton broth media and incubated overnight at 37 °C. This procedure is used to verify the absence of bacteria when none are detected by plating. A Vitek 2 automated system (bioMérieux) was used for biochemical identification of all isolates growing on the agar media, in order to verify that no unwanted contamination occurred during implantation or explantation.

### 2.17. Statistical analysis

Statistical analysis was performed using the GraphPad Software (San Diego, CA). Values are given as mean  $\pm$  SEM. Comparison between several groups used two-way ANOVA followed by Bonferroni post-test. Statistical significance was set up at  $P < 0.05$ .

## 3. Results

### 3.1. Characterization of EO-sterilized coated substrates

The surface of the Ti-SAg EO sample was characterized using water contact angle, XPS and ToF-SIMS measurements. The average water contact angle value for Ti-SAg EO ( $93 \pm 2^\circ$ ) was identical to the value for Ti-SAg samples ( $92 \pm 3^\circ$ ) [27]. XPS analysis of Ti-SAg EO indicated the presence of the expected elements P, C, S and Ag on the Ti surfaces. The atomic surface composition is given in Table 1. The P/S and Ag/S ratios were consistent with the theoretical ratio of 1, expected for the formation of silver thiolate groups (Fig. 1). The C/S ratio was significantly higher than the theoretical ratio of 12, indicating a contamination by hydrocarbons. The high-

**Table 1**  
Atomic percentages and ratios derived from XPS analysis for MDP/AgNO<sub>3</sub>-coated Ti sterilized by ethylene oxide (Ti-SAg EO).

	C (at.%)	S (at.%)	P (at.%)	Ag (at.%)	C/S	P/S	Ag/S
Ti-SAg EO	36.4 $\pm$ 2.6	1.4 $\pm$ 0.3	1.9 $\pm$ 0.3	1.1 $\pm$ 0.3	26.0	1.3	0.8

resolution S2p scan (Fig. 2A) showed doublet S2p peaks ( $S2p_{1/2}$  and  $S2p_{3/2}$ ) with a split of 1.2 eV and a 2:1 peak area ratio. Deconvolution showed the presence of three different doublets, at about 168.2, 164.0 and 162.2 eV, ascribed respectively to oxidized sulfur species (likely linked to silver, e.g.  $RSO_xAg$ ), unbound thiol or disulfide (SH or SS) groups and silver thiolate (SAG) species, respectively. The percentage of each species is given in Table 2. The surface composition of the Ti-SAG EO sample showed a lower percentage of RSAG species and a higher percentage of  $RSO_x$  species compared to our previous report [27]. EO is not an oxidant [43], and thus this high level of oxidized species has to be related to the high sensitivity of silver thiolate bonds to oxidation [44,45]. In the present work, due to delays imposed by the sterilization pro-

**Table 2**

Peak fitting parameters and per cent peak areas for the S2p high-resolution spectra of Ti-SAG EO sample.

Sample	BE <sup>a</sup> (eV)	FWHM <sup>b</sup> (eV)	% Area	Attribution
Ti-SAG EO	162.2	2.0	17	Silver thiolates
	164.0	1.5	19	Thiols, disulfides
	168.2	2.0	64	Oxidized sulfur species

<sup>a</sup> Binding energy.

<sup>b</sup> Full width at half-maximum.

cedure and access to XPS equipment, the time between synthesis and XPS characterization was ~2 months compared to ~2 weeks

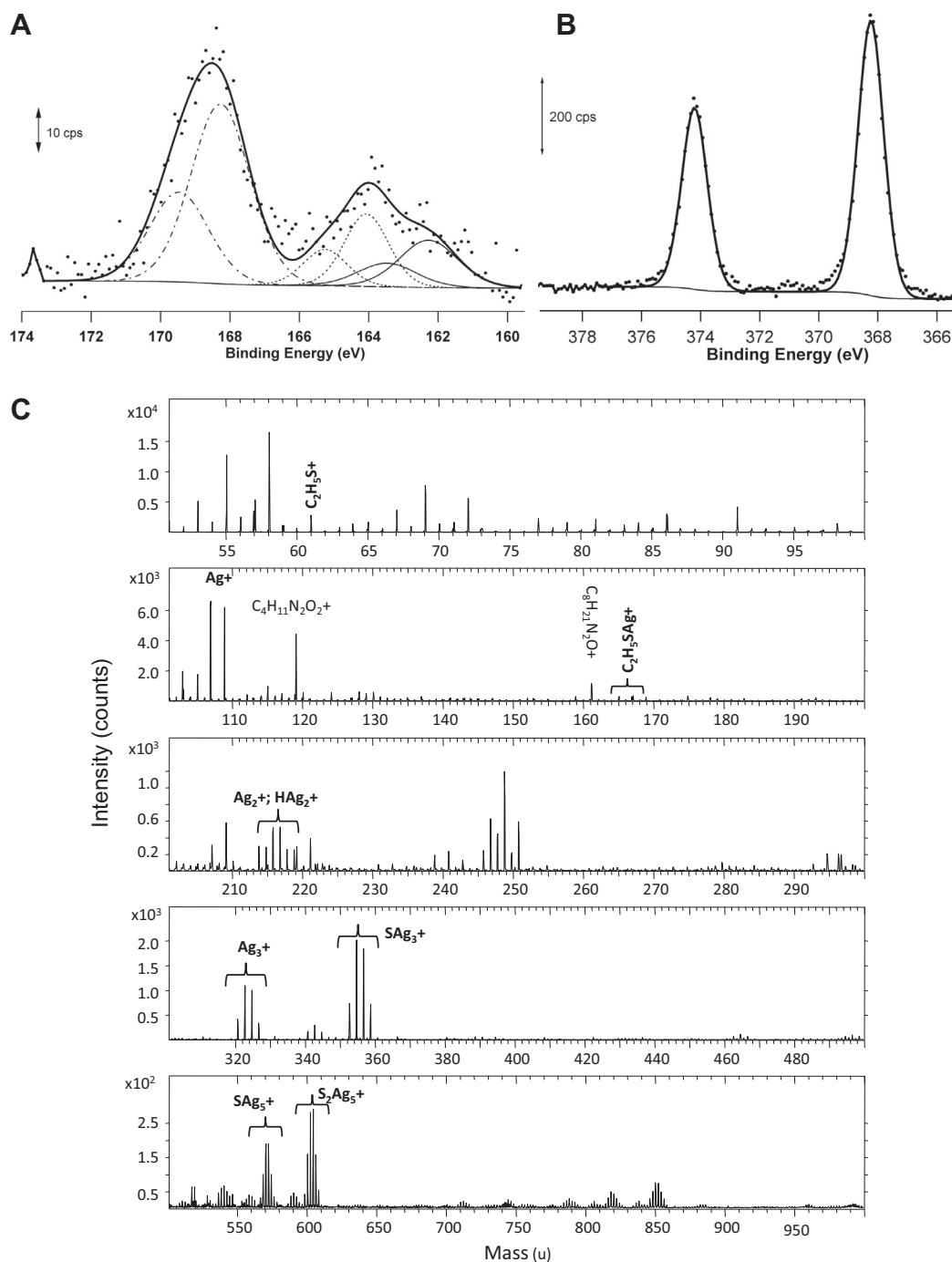


**Fig. 2.** Surface characterization of MDPA/AgNO<sub>3</sub>-coated Ti plates. (A) High-resolution XPS S2p spectrum. (B) High-resolution Ag3d spectrum. (C) Positive ToF-SIMS spectrum.

in our former work. In the case of dodecylthiol SAMs on silver, Schoenfish and Pemberton found that nearly 50% of silver thiolate bonds were converted to sulfonate species after exposure to ambient air for 1 week [44]. Traces of ozone in ambient air were identified as the primary oxidant. The Ag3d XPS peaks are not sensitive to the degree of oxidation of Ag [46,47], and in spite of the various silver environments (SAg, SO<sub>x</sub>Ag) suggested by the S2p spectrum, the high-resolution Ag3d spectrum of Ti-SAg EO (Fig. 2B) showed a single doublet (Ag3d<sub>5/2</sub> and Ag3d<sub>3/2</sub>) at a binding energy of 367.7 eV (Ag3d<sub>5/2</sub>), similar to the binding energy reported for Ag<sup>0</sup> or Ag<sup>+1</sup> in Ag<sub>2</sub>S (367.8 eV), bulk silver (368.2 eV), layered silver dodecylthiolate (368.2 eV), or silver colloids capped by a dodecylthiol monolayer (368 eV) [46].

ToF-SIMS analysis was used to provide qualitative information on the species present at the outermost surface of the samples. The surface of non-modified Ti samples was contaminated by various hydrocarbons (ions C<sub>x</sub>H<sub>y</sub><sup>-</sup>) and N-containing compounds (ions C<sub>x</sub>H<sub>y</sub>N<sup>+</sup>, C<sub>x</sub>H<sub>y</sub>O<sub>z</sub>N<sub>t</sub><sup>+</sup>), but also by oxidized sulfur species (ions SO<sub>x</sub><sup>-</sup>) as well as oxidized phosphorus species (ions PO<sub>x</sub><sup>-</sup>, CaPO<sub>2</sub><sup>-</sup>). Halogens (Cl<sup>-</sup>, F<sup>-</sup>, Br<sup>-</sup>, I<sup>-</sup>), alkali metals (Na<sup>+</sup>, K<sup>+</sup>) and alkaline earth metals (Ca<sup>+</sup>, Mg<sup>+</sup>) were also detected. The main Ti-containing ions, characteristic of the substrate, were <sup>48</sup>Ti<sup>+</sup> (m/z 47.95), <sup>48</sup>HTi<sup>+</sup> (m/z 48.96), TiO<sup>+</sup> (m/z 63.94) or HTi<sub>2</sub>O<sub>5</sub><sup>-</sup> (m/z 176.87). Importantly, no silver was detected on the unmodified Ti samples. The Ti-containing ions were much less intense in the spectra of Ti-SAg EO, due to the masking effect of the coating, whereas numerous Ag- and/or S-containing ions were detected. Ion fragments characteristic of the MDPA/Ag monolayer are listed in Table 3. In positive mode, the spectrum of Ti-SAg EO (Fig. 2C) showed that the surface was contaminated by N-containing compounds (ions C<sub>x</sub>H<sub>y</sub>N<sup>+</sup> and C<sub>x</sub>H<sub>y</sub>O<sub>z</sub>N<sub>t</sub><sup>+</sup>). The presence of Ag at the extreme surface of the samples was attested by the numerous Ag-containing ions detected. In these ions, silver is often bonded to sulfur (Ag<sub>x</sub><sup>+</sup> and S<sub>x</sub>Ag<sub>y</sub><sup>+</sup> ions). The high intensity of ions containing several Ag atoms (with characteristic patterns due to the two main Ag isotopes <sup>107</sup>Ag and <sup>109</sup>Ag) suggests the presence of Ag–Ag bonds in addition to SAg bonds. Low-intensity fragments characteristic of MDPA were also detected, such as C<sub>2</sub>H<sub>5</sub>S<sup>+</sup> (m/z = 61.01). The spectrum in negative mode of Ti-SAg EO showed abundant sulfur-containing ions, often combined to silver. In addition, a contamination by iodine (I<sup>-</sup> ion at m/z 126.90) and bromine (<sup>79</sup>Br<sup>-</sup> ion at m/z 78.92, overlapped by PO<sub>3</sub><sup>-</sup> at m/z 78.96 and <sup>79</sup>Br<sup>-</sup> ion at m/z 80.97) was detected. This contamination led to various Ag-containing ions with characteristic isotope patterns, such as AgI<sub>2</sub><sup>-</sup> (doublet at m/z 360.74 and 362.71), SAgI<sup>-</sup> (doublet at m/z 265.78 and 267.78), AgBr<sub>2</sub><sup>-</sup> (quadruplet between 264.74 and 268.84), SAgBr<sup>-</sup> and SHAgBr<sup>-</sup> (overlapping triplets between m/z 217.79 and 222.85).

**Table 3**  
Characteristic secondary ions containing S and/or Ag atoms detected at the surface of the Ti-SAg EO sample.

Negative ions		Positive ions	
Attribution	m/z	Attribution	m/z
S <sup>-</sup>	31.97	C <sub>2</sub> H <sub>5</sub> S <sup>+</sup>	61.01
SH <sup>-</sup>	32.98	( <sup>107</sup> Ag) <sup>+</sup>	106.91
S( <sup>107</sup> Ag) <sup>-</sup>	138.88	C <sub>2</sub> H <sub>4</sub> S( <sup>107</sup> Ag) <sup>+</sup>	166.91
HS( <sup>107</sup> Ag) <sup>-</sup>	139.89	( <sup>107</sup> Ag) <sub>2</sub> <sup>+</sup>	213.81
S <sup>107</sup> Ag <sup>79</sup> Br <sup>-</sup>	217.80	H( <sup>107</sup> Ag) <sub>2</sub> <sup>+</sup>	214.82
HS <sup>107</sup> Ag <sup>79</sup> Br <sup>-</sup>	218.80	( <sup>107</sup> Ag) <sub>3</sub> <sup>+</sup>	320.72
S <sub>2</sub> <sup>107</sup> Ag <sup>79</sup> Br <sup>-</sup>	249.77	S( <sup>107</sup> Ag) <sub>3</sub> <sup>+</sup>	352.69
<sup>107</sup> Ag <sup>79</sup> Br <sub>2</sub> <sup>-</sup>	264.74	HS( <sup>107</sup> Ag) <sub>4</sub> <sup>+</sup>	460.60
S <sup>107</sup> AgI <sup>-</sup>	265.78	( <sup>107</sup> Ag) <sub>5</sub> <sup>+</sup>	534.53
<sup>107</sup> Ag <sup>79</sup> BrI <sup>-</sup>	312.73	S( <sup>107</sup> Ag) <sub>5</sub> <sup>+</sup>	566.50
S <sup>107</sup> Ag <sub>2</sub> <sup>79</sup> Br <sup>-</sup>	324.70	S <sub>2</sub> ( <sup>107</sup> Ag) <sub>5</sub> <sup>+</sup>	598.47
<sup>107</sup> AgI <sub>2</sub> <sup>-</sup>	360.72		
S <sup>107</sup> Ag <sub>2</sub> I <sup>-</sup>	372.69		

Therefore, after EO sterilization and storage, the MDPA/AgNO<sub>3</sub> nanocoatings can be described as phosphonate monolayers terminated by different sulfur species (sulfonate, thiol/disulfide, thiolate) interacting with silver ions and small silver clusters or polymers.

### 3.2. In vitro antibacterial activity of coatings

Sterilization of medical devices is compulsory for clinical applications. Sterilization by EO is a well-known sterilization method, well suited to sensitive medical devices [43]. In order to evaluate the influence of EO sterilization on the antibacterial activity of the MDPA/AgNO<sub>3</sub> coatings, we examined the bacterial adhesion after 2 h and the biofilm formation at 3 days on unmodified and modified Ti substrates, without or with EO sterilization, using two bacterial strains: *E. coli* ATCC 25922 and *S. epidermidis* ATCC 12228. For both strains, the adhesion assay (Fig. 3A) showed that the antibacterial efficiency of the coating was maintained after EO sterilization. The number of viable adherent bacteria on the coated samples (Ti-SAg and Ti-SAg EO) was decreased by at least 3 orders of magnitude as compared to the uncoated Ti substrates (Ti and Ti EO). Similarly, the density of biofilm (Fig. 3B) on Ti-SAg and Ti-SAg EO was ~80% lower for both bacterial strains than on Ti and Ti EO substrates.

Further information on the mechanism of action of the MDPA/AgNO<sub>3</sub> coating was obtained by monitoring the viability of the bacteria adhering to the samples after incubation for 2 h (LIVE/DEAD assay). Irrespective of the bacterial strain, fluorescence microscopy images (Fig. 3C–F) showed that the Ti EO samples were completely covered by a dense layer of live adherent bacteria (green fluorescence). Conversely, no viable adherent bacteria were detected at the surface of the Ti-SAg EO samples, which showed only a few non-viable adherent bacteria (red fluorescence), indicating that the MDPA/AgNO<sub>3</sub> coating not only killed adherent bacteria but also prevented adhesion of dead bacteria. These results confirm the significant antibacterial activity of the MDPA/AgNO<sub>3</sub> coating and demonstrate that this activity is fully maintained after EO sterilization.

### 3.3. Cytotoxicity of AgNO<sub>3</sub> and/or MDPA solutions

The antibacterial monolayers described here involve the use of MDPA and AgNO<sub>3</sub>. The cytotoxicity of MDPA or/and AgNO<sub>3</sub> in solution was evaluated by measuring their effect on cell growth using the established cell line MC3T3-E1. These cells are derived from newborn mice calvaria [48] and are commonly used as an in vitro model of osteoblast development [49]. The first test consisted in the quantification of cells after 4 days of culture in medium containing increasing concentrations of MDPA, AgNO<sub>3</sub> or a mixture of both compounds. This dose–response analysis indicated that AgNO<sub>3</sub> was strongly toxic at 3 mg l<sup>-1</sup>, but not at lower concentrations (Fig. 4A). MDPA showed no toxicity up to 3 mg l<sup>-1</sup> when used alone. Interestingly, MDPA/AgNO<sub>3</sub> mixtures showed lower toxicity at 3 mg l<sup>-1</sup> than AgNO<sub>3</sub> at the same concentration. Time-course analyses confirmed these findings: at 3 mg l<sup>-1</sup> AgNO<sub>3</sub> was toxic as early as day 1 and significantly at day 4 (Fig. 4B), while MDPA/AgNO<sub>3</sub> mixtures were less toxic than pure AgNO<sub>3</sub>. At 1 mg l<sup>-1</sup> (Fig. 4C), no toxicity was noted, independently of the compound and of the time.

### 3.4. Adhesion and proliferation of MC3T3-E1 on Ti substrates

In a second step, the potential cytotoxicity of the coating was directly assessed by seeding MC3T3-E1 cells on the different Ti substrates. Data indicated that MC3T3-E1 cells proliferated equally well at the surface of Ti, Ti-SAg, Ti-SAg EO and cell culture treated

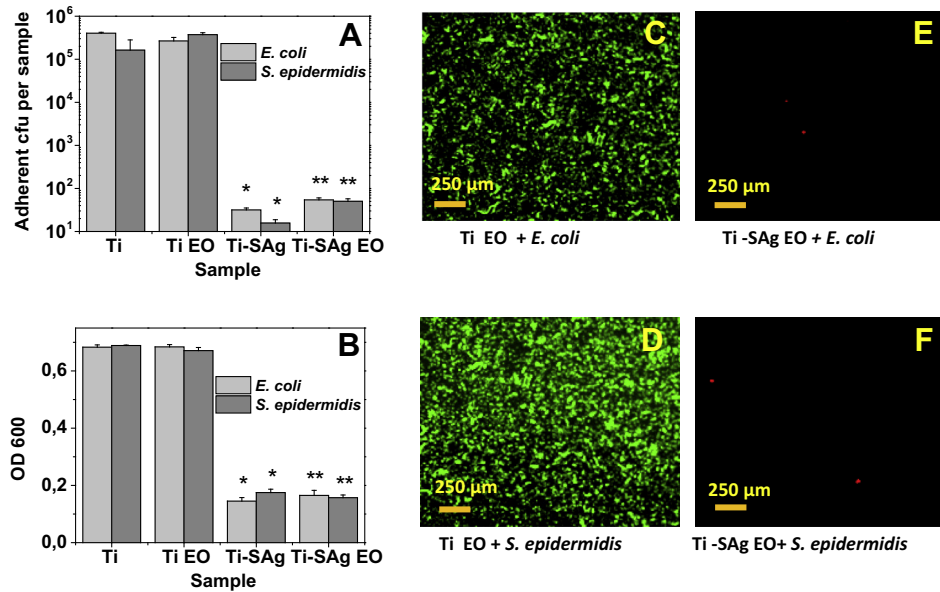


**Fig. 3.** Influence of the MDP/AgNO<sub>3</sub> monolayer and of EO sterilization on bacterial adhesion and biofilm formation. (A) Number of viable adherent bacteria after incubation for 2 h. \**P* < 0.05 vs. Ti. (B) Biofilm density quantified by colorimetry after incubation for 72 h. \**P* < 0.05 vs. Ti. (C–F) Viability of adherent bacteria assessed by fluorescence imaging: (C) Ti EO + *E. coli* 25922, (D) Ti EO + *S. epidermidis* 12228, (E) Ti-SAg EO + *E. coli* 25922 and (F) Ti-SAg EO + *S. epidermidis* 12228.

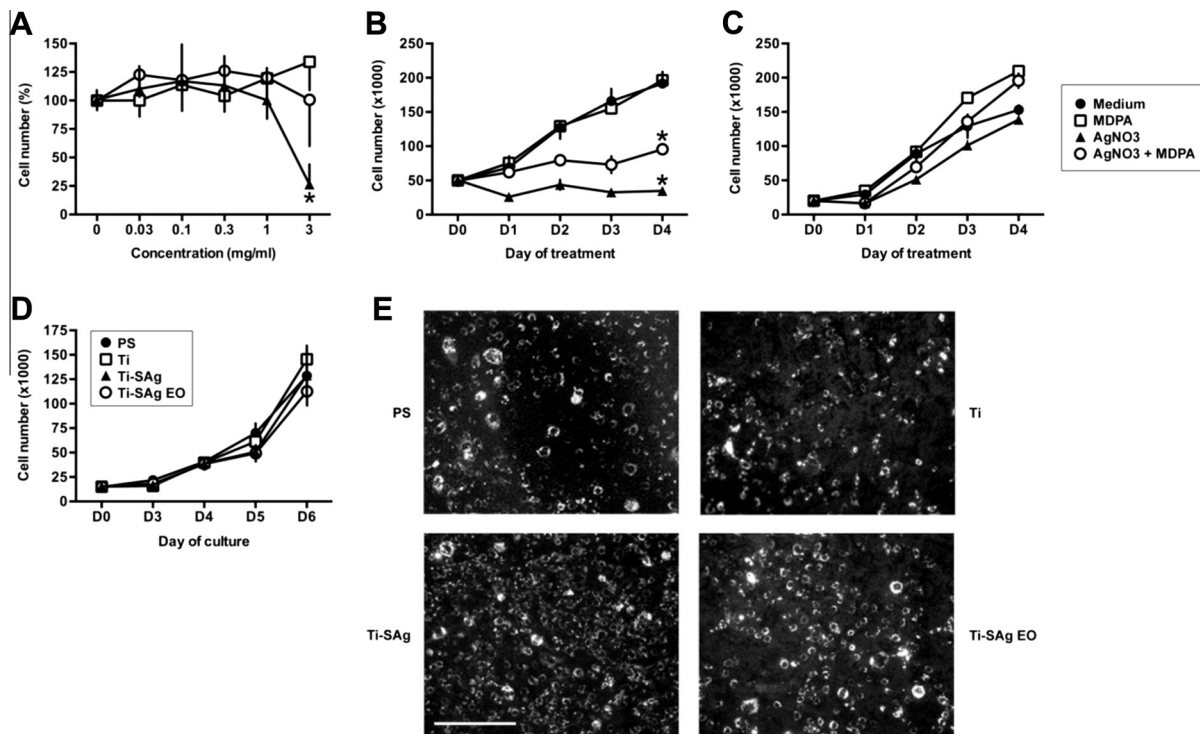


**Fig. 4.** Effect of MDP and AgNO<sub>3</sub> solutions, and of MDP/AgNO<sub>3</sub> coating on the growth of MCT3T3 cells. (A) Cells were cultured for 4 days with increasing concentrations of compounds as indicated (symbols are described on the right of panel C). Cell number is expressed as percentage of that found in untreated control. \**P* < 0.05 vs. control. (B) Effect of 3 mg/L of MDP or/and AgNO<sub>3</sub> on cell growth. \**P* < 0.05 vs control. (C) Effect of 1 mg l<sup>-1</sup> of MDP or/and AgNO<sub>3</sub> on cell growth. (D) Cell proliferation on plastic dishes (PS), uncoated Ti (Ti), MDP/AgNO<sub>3</sub>-coated Ti (Ti-SAg) or sterilized Ti-SAg (Ti-SAg EO). (E) Fluorescence microscopy images showing cultures at day 4. Scale bar = 100 μm.

polystyrene (Fig. 4D) during a 6-day period. Fluorescence microscopy (Fig. 4E) showed that the cells had adhered to and spread over the various Ti substrates and the cell culture treated polystyrene surface in a similar way, indicating the non-harmful effect of the monolayers, before or after EO sterilization, toward MC3T3-E1 cell proliferation.

### 3.5. Osteogenic differentiation on Ti substrates

We next investigated whether the surface modification of Ti interfered with osteogenic differentiation. To this purpose, MC3T3-E1 cells and murine MSCs were seeded on the different substrates and cultured in osteoinductive medium. Cells cultured

in proliferative medium on tissue culture treated plastic dishes served as undifferentiated control. For both cell lines, expression of the osteogenic markers Osteocalcin and Runx2 was up-regulated after culture on non-modified and on modified Ti substrates to a similar or sometimes higher degree as compared to culture on plastic dishes (Fig. 5A). Furthermore, EO sterilization of the modified Ti substrate did not alter the capacity of cells to commit osteogenic differentiation (Fig. 5A). To further evaluate differentiation of MSCs into osteoblasts, we examined their capacity to mineralize and produce alkaline phosphatase activity. When the cells were cultured in differentiation medium, calcium deposits appeared on all substrates as shown by Alizarin Red S staining (Fig. 5B). Spectrophotometry indicated that mineralization occurred as efficiently on Ti-SAg EO substrate as on unmodified Ti (Fig. 5C). The cells also produced similar levels of alkaline phosphatase activity on both substrates (Fig. 5D). These data show that neither the coating nor the EO sterilization procedure affected the differentiation and mineralization processes.

### 3.6. *In vivo* cytocompatibility of functionalized Ti discs

We then investigated the *in vivo* cytocompatibility of sterilized Ti samples. To evaluate the survival of cells in contact with unmodified or functionalized Ti discs, we used the C3-Luc MSC line that expresses the luciferase gene. After subcutaneous implantation of discs coated with C3-Luc cells in SCID/Bg mice, the bioluminescent signal was monitored at different time points. As a control, C3-Luc cells were injected subcutaneously in SCID/Bg mice. Photon emission, which is related to the luciferase activity of C3H-Luc and is proportional to the number of live cells, was recorded as pseudocolor images (Fig. 6A). Quantification of the luminescent signals revealed that at day 1, the signal from injected C3-Luc cells in the control was significantly higher than the one measured with the cells seeded on the Ti discs (Fig. 6B), but there was no difference whether the discs were functionalized or not. From day 2 to day 4, the luminescent signals decreased, indicative of cell death. Nevertheless, the signal intensities were similar in the control and implanted groups of mice, indicating that the survival of cells was not affected by contact with the implants and demonstrating the cytocompatibility of Ti-SAg EO functionalized samples.

### 3.7. *In vivo* tolerance of functionalized Ti discs

Tolerance of immunocompetent mice to subcutaneous implantation of Ti EO or Ti-SAg EO discs was assessed after 7 and 21 days. Macroscopic examination of tissues surrounding the implants revealed the presence of connective and fat tissues after 7 and 21 days (Fig. 7A, B). The surrounding connective tissues appeared vascularized with little indication of residual inflammation. Tissues adhering to the implants were then processed for routine histology and hematoxylin/eosin staining. Histological analysis confirmed the presence of mostly fibrous and fat tissues, as well as blood vessels at day 7, in mice implanted with Ti EO or Ti-SAg EO implants. In some locations, mild signs of inflammation were observed but no severe immune response due to implant rejection was recorded (see arrows, Fig. 7C, D). At day 21, similar observations were made for both types of implants (data not shown). Accordingly, both Ti-SAg EO and non-modified Ti EO implants were well tolerated.

### 3.8. *In vivo* antibacterial activity of Ti-SAg EO implants

The antibacterial activity of the MDPA/AgNO<sub>3</sub> coating was then evaluated *in vivo*. Ti EO and Ti-SAg EO discs were implanted subcutaneously in the back of immunocompetent mice. Then  $1 \times 10^4$  cfu of *S. epidermidis* in 50  $\mu$ l of PBS were injected directly onto the disc surface. After 14 days, quantification of viable adherent bacteria

on the discs (Table 4) indicated the presence of numerous *S. epidermidis* bacteria on the uncoated Ti EO discs whereas very few bacteria were retrieved on the coated Ti-SAg EO discs. The more than 500-fold reduction in the number of viable adherent bacteria found demonstrates, under the conditions used here, the excellent antibacterial efficiency of the MDPA-AgNO<sub>3</sub> monolayers *in vivo*.

## 4. Discussion

The major result of this study is that nanocoatings based on MDPA monolayers post-functionalized by AgNO<sub>3</sub> and sterilized by EO exhibit excellent antibacterial activity and biocompatibility, both *in vitro* and *in vivo*. This finding underlines that a minimal amount of silver located at the outermost surface of a biomaterial can confer significant antibacterial activity, even *in vivo*, while avoiding any toxicity issues.

Silver is the most used antiseptic agent in antibacterial coatings due to its broad antibacterial spectrum, inhibition of bacterial adhesion and low risk of bacterial resistance [7,8,11,35]. Several *in vivo* studies have demonstrated that silver-containing coatings may help reduce the risk of infection on implants [50–54]. However, the biocompatibility of silver-containing coatings is still debated, particularly in the case of silver nanoparticles (Ag NPs). For instance, Zhao et al. [55] and De Giglio et al. [56] reported some cytotoxicity toward osteoblasts of coatings incorporating Ag NPs. Conversely, Liu et al. found that Ag NPs in PLGA films promoted proliferation and maturation of preosteoblasts *in vitro* [53]. These discrepancies are probably due to the fact that the amount of silver ions released from Ag NPs, and thus their antimicrobial activity and cytotoxicity, depends on several factors, including the size and shape of the nanoparticles, their capping chemistry, the culture conditions, and the bacterial strain or cell line. In most cases, the total silver loading in silver-containing antibacterial coatings is much higher than the toxic level for human cells. Accordingly, the silver ion release must be carefully tuned in order to ensure sufficient antibacterial activity while avoiding toxicity to mammalian cells [38,52,57–60]. Alternatively, the loading of silver in the film can be decreased to ensure that even if all the silver was released in the medium, the level toxic for mammalian cells cannot be reached.

In our approach, the amount of silver in the coating is limited by the initial amount of thiol groups in the MDPA monolayer: one thiol group can react with one Ag<sup>+</sup> ion only, as confirmed by the experimental Ag/S ratio measured by XPS, which is close to 1. Thus, based on the typical density of alkylphosphonic acid molecules in SAMs ( $4 \pm 1$  molecule nm<sup>-2</sup>) [61,62], the maximum silver loading in our coating is estimated to be  $\sim 0.65 \pm 0.15$  nmol cm<sup>-2</sup> or  $70 \pm 20$  ng cm<sup>-2</sup>. To understand the origin of the biocompatibility of the MDPA/AgNO<sub>3</sub> monolayer, we evaluated the cytotoxicity of AgNO<sub>3</sub> solutions on preosteoblasts: a significant cytotoxic effect was observed at 3 mg l<sup>-1</sup> (17.8  $\mu$ mol l<sup>-1</sup>), but no toxicity was found for a concentration of 1 mg l<sup>-1</sup> (6.0  $\mu$ mol l<sup>-1</sup>). If all the silver present at the surface of our samples (2 cm<sup>2</sup>) was released in the medium (0.5 ml) during the *in vitro* cytotoxicity assay, the maximum silver concentration would be  $2.6 \pm 0.5$   $\mu$ mol l<sup>-1</sup> (0.28  $\pm$  0.6 ppm) and should not lead to any cytotoxicity. It is thus not surprising that the MDPA/AgNO<sub>3</sub> monolayers did not hinder the adhesion and proliferation of MC3T3-E1 or alter the capacity of MC3T3-E1 cells and MSCs to commit osteogenic differentiation. Importantly, these monolayers did not modify the *in vivo* biocompatibility of Ti implants, as shown using a longitudinal analysis of luciferase-expressing cells in direct contact with the implants and by histological examination of the retrieved implants.

Despite their very low silver loading and although the S-Ag bonds were largely oxidized to SO<sub>x</sub>-Ag during storage, the

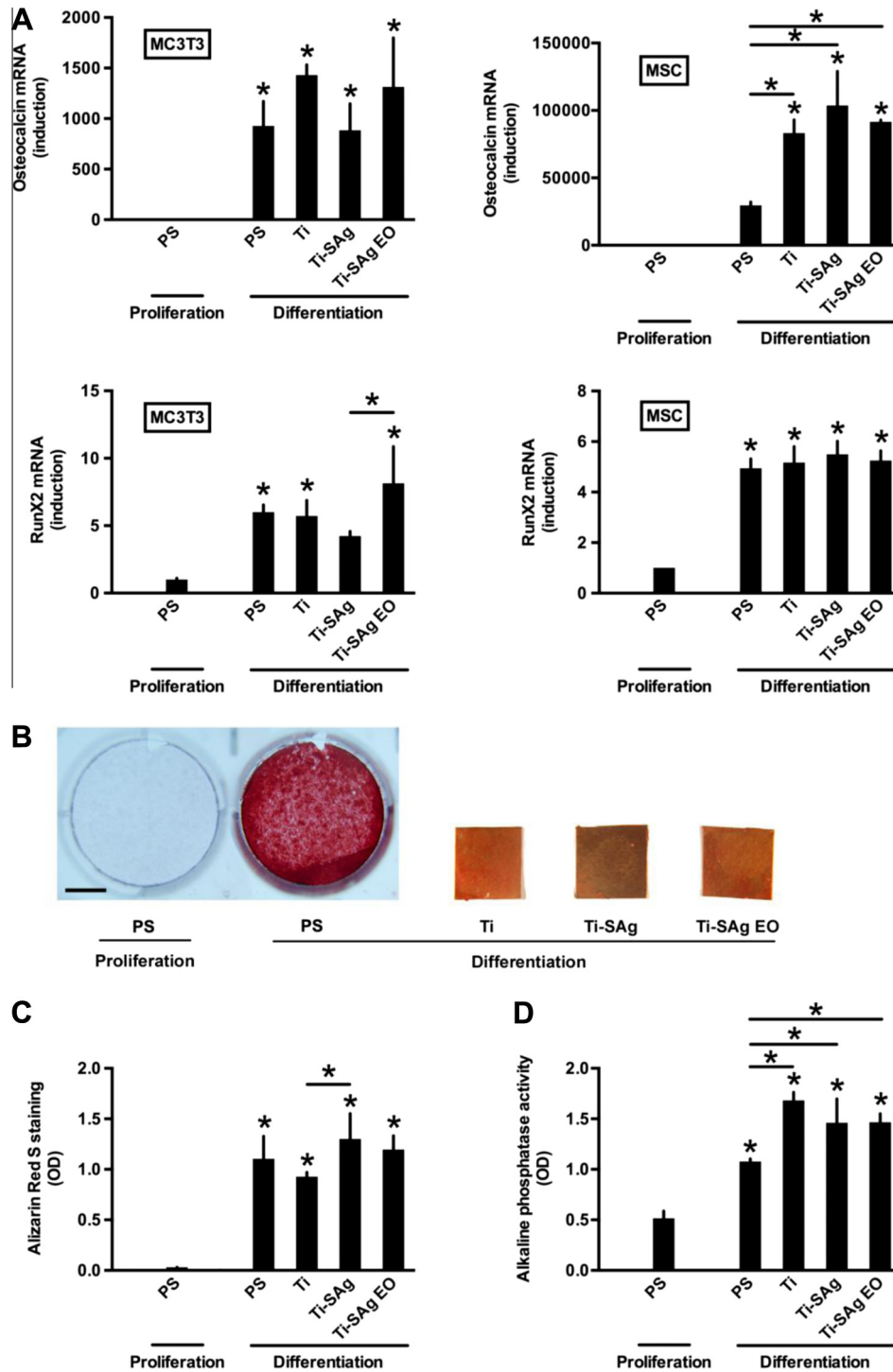


**Fig. 5.** Osteogenic differentiation on Ti plates. MC3T3 cells and MSCs were cultured in differentiation medium either on plastic dishes (PS) or on uncoated Ti (Ti), MDPA/AgNO<sub>3</sub>-coated Ti (Ti-SAg) or sterilized Ti-SAg (Ti-SAg EO). Cells cultured on PS in proliferation medium served as undifferentiated control. (A) Expression of osteocalcin and RunX2 was analyzed by RT-qPCR. (B) Alizarin Red S staining of MSCs showing calcium deposits (orange-red color). Bar = 1 cm. (C) Quantification of solubilized Alizarin Red S staining. (D) Alkaline phosphatase activity secreted by MSCs. \**P* < 0.05 vs. PS in proliferation condition or between two substrates when indicated by a bar.

MDPA/AgNO<sub>3</sub> coatings efficiently inhibited bacterial adhesion and biofilm formation of both *E. coli* and *S. epidermidis* strains. LIVE/DEAD staining indicated the presence of a low density of dead bacteria at the surface of the coated samples, suggesting that the MDPA/AgNO<sub>3</sub> coating killed adherent bacteria but also prevented bacterial adhesion, presumably by damaging bacteria before adhesion to the coated surface. Importantly, we found a significant in vivo antibacterial effect of the MDPA/AgNO<sub>3</sub> monolayer, with a

more than 500-fold reduction in the number of *S. epidermidis* bacteria recovered after a 2 week period on the coated implants compared to uncoated implants. Owing to the limited stability of phosphonate monolayers as well as silver thiolate bonds in biological media [27,63], and considering their extremely low silver content, these monolayers are not intended to provide long-term protection against bacteria. However, the present results indicate that MDPA/AgNO<sub>3</sub> monolayer could be used on medical devices

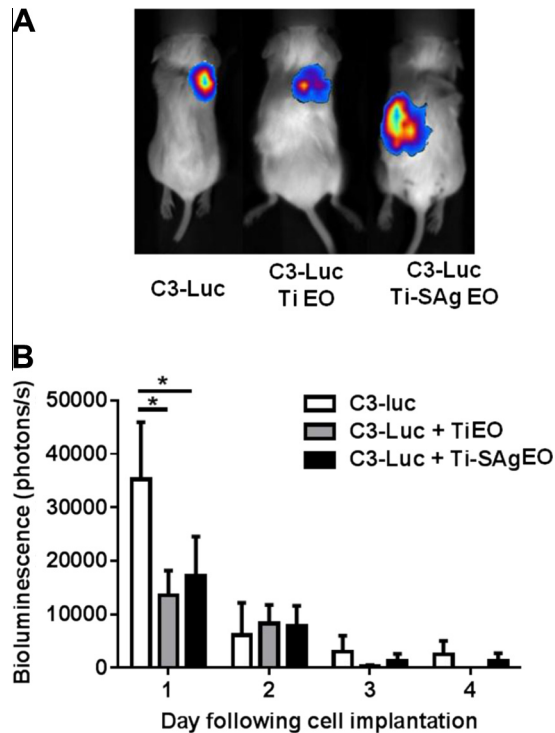


**Fig. 6.** Cytocompatibility of sterilized uncoated (Ti EO) or MDPA/AgNO<sub>3</sub>-coated (Ti-SAg EO) Ti discs. C3-Luc cells were cultured on the surface of Ti EO or Ti-SAg EO discs for 5 h and implanted subcutaneously into SCID/Bg mice. As a control, C3-Luc cells were injected subcutaneously. Survival of cells was evaluated by in vivo bioluminescence imaging. (A) Representative picture obtained at day 1 post-injection. (B) Survival of C3-Luc cells as measured from day 1 to day 4 after implantation. Data are expressed as mean fluorescence intensity in photons s<sup>-1</sup> ± SEM, \*P < 0.05.

to hinder microbial adhesion and biofilm growth at the device surface in the first few days following implantation, thus favoring tissue integration in the “race for the surface” [64].

A few recent publications have also evidenced the in vitro antibacterial efficiency of coatings involving submicrogram amounts of silver per cm<sup>2</sup>. These coatings were based on completely different approaches, and the antibacterial efficiency was not investigated in vivo. For instance, Agarwal et al. [37] described antibacterial polymeric thin films (<100 nm) prepared by layer-by-layer deposition and loaded with as little as 0.39 ± 0.03 μg cm<sup>-2</sup> of silver that were bactericidal for *S. epidermidis*, leading to a 6 log<sub>10</sub> reduction in the number of viable bacteria in suspensions contacted for 8 h with the films. The films with a silver loading of 0.39 ± 0.03 μg cm<sup>-2</sup> were not cytotoxic, allowing attachment and growth of murine fibroblasts (NIH-3T3) cells, whereas films with only slightly higher loadings (>0.58 ± 0.04 μg cm<sup>-2</sup>) showed measurable cytotoxicity. Pallavicini et al. [33] investigated monolayers of Ag nanoparticles anchored to glass substrates via a mercaptopropyltrimethoxysilane layer, with a total silver loading of 0.357 μg cm<sup>-2</sup>. They found a 5 log<sub>10</sub> reduction in the number of viable bacteria (*E. coli* and *S. aureus*) contacted for 24 h with modified glass substrates, even though the Ag release was very slow, reaching only ~15% of the initial Ag amount after 19 days. However, they did not investigate the cytotoxicity of their coatings. Marsich et al. [65] described a nanocomposite antimicrobial coating formed by a chitosan derivative and Ag NPs. Coatings on thermosets with a surface silver content of 0.096 ± 0.031 μg cm<sup>-2</sup> showed good anti-bacterial and anti-biofilm activity, with a 6 log<sub>10</sub> reduction in the number of viable bacteria (*E. coli* and *S. aureus*) seeded on the substrates after 3 h incubation. In vitro tests showed that the coating did not hamper differentiation of mesenchymal cells in osteoblasts under osteogenic conditions, and in vivo tests

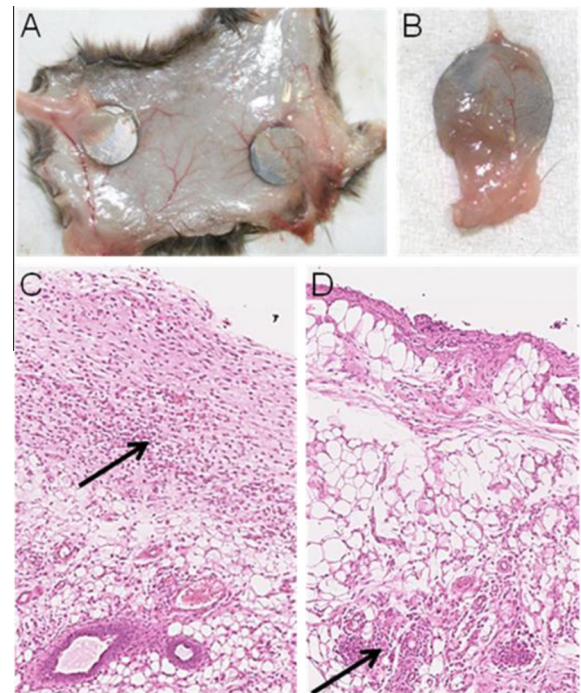


**Fig. 7.** Biotolerance of sterilized uncoated (Ti EO) or MDPA/AgNO<sub>3</sub>-coated (Ti-SAg EO) Ti discs. The discs were implanted subcutaneously into DBA1 mice for 7 or 21 days and tissue surrounding the implants were processed for histology. (A) Representative macroscopic view of Ti EO and Ti-SAg EO discs (left and right, respectively) at day 7 after implantation. (B) Same Ti-SAg EO disc as in (A), at higher magnification. (C) Representative histological image of tissues adjacent to Ti EO discs after hematoxylin/eosin staining at day 7 (magnification ×5). (D) Representative histological image of tissues adjacent to Ti-SAg EO discs after hematoxylin/eosin staining at day 21 (magnification ×5). Arrow: mild signs of inflammation.

**Table 4**

Number of viable adherent bacteria found on the Ti EO and Ti-SAg EO substrates 14 days after implantation, suture and subcutaneous injection of ~10<sup>4</sup> cfu of *S. epidermidis* ATCC 12228 on the substrate.

Sample	Mouse	No. of colonies (cfu per sample)
Ti EO	A	6.3 × 10 <sup>4</sup>
	B	1.8 × 10 <sup>4</sup>
	C	3.5 × 10 <sup>4</sup>
	D	8.1 × 10 <sup>4</sup>
	E	2.2 × 10 <sup>4</sup>
Ti-SAg EO	F	20
	G	0
	H	0
	I	30
	J	0

showed good biological compatibility of the coated materials when implanted in bony tissue.

The results obtained in the present study confirm the interest of coating strategies involving very low amounts of silver in thin films to prevent bacterial colonization on implants while ensuring good biocompatibility. We show in addition that a routine (standard) sterilization procedure used for medical devices did not affect the biocompatibility and antibacterial properties of our monolayer. Moreover, our monolayer retained a significant antibacterial efficiency in vivo, indicating the viability of this approach for clinical applications.

## 5. Conclusions

In this study, the antibacterial efficiency and biocompatibility of monolayers based on the grafting onto titanium substrates of

MDPA self-assembled monolayers post-reacted with AgNO<sub>3</sub> was demonstrated in vitro and in vivo. In vitro, the MDPA/AgNO<sub>3</sub> monolayers significantly inhibited *E. coli* and *S. epidermidis* adhesion and biofilm formation while allowing attachment and proliferation of MC3T3-E1 preosteoblasts. After sterilization by ethylene oxide and storage under argon, XPS and ToF-SIMS showed that the nano-coatings can be described as phosphonate monolayers terminated by different sulfur species (sulfonate, thiol/disulfide, thiolate) interacting with silver ions and small silver clusters or polymers. Importantly, both antibacterial activity and biocompatibility were maintained after sterilization. Osteogenic differentiation of MC3T3 cells and murine MSCs was not affected by the coatings. Furthermore, we demonstrated in vivo the excellent biocompatibility of sterilized MDPA/AgNO<sub>3</sub>-coated Ti implants and their antibacterial activity against *S. epidermidis*. These results may be ascribed to the minimal silver loading ( $\sim 0.65$  nmol Ag cm<sup>-2</sup>) exposed at the extreme surface of the monolayer. Phosphonic acid monolayers can be used to modify a wide range of metallic and ceramic substrates, simply by immersion in an ethanol or a water solution. This approach can thus be readily extended to the prevention of bacterial adhesion and biofilm formation on metallic (e.g. Ti alloys, stainless steel or Co–Cr alloys) and ceramic (e.g. alumina, zirconia) devices.

### Acknowledgements

M.M. and D.N. thank Maxime Gasnier for technical assistance. This work was supported by INSERM and CNRS, the Universities of Montpellier 1 and Montpellier 2, the Languedoc-Roussillon Region and the European Regional Development Fund (FEDER N° 41484). We thank the Agence Nationale pour la Recherche for support of the national infrastructure: “ECELLFRANCE: Development of a national adult mesenchymal stem cell based therapy platform” (ANR-11-INSB-005). We also thank the “Réseau des Animaleries de Montpellier” animal facility and the “Réseau d’Histologie Expérimentale de Montpellier” histology facility for processing our animal tissues and the “Montpellier RIO Imaging” platform. The authors confirm that there are no known conflicts of interest associated with this publication.

### Appendix A. Figures with essential color discrimination

Certain figures in this article, particularly Figs. 3, 5, 6, and 7, are difficult to interpret in black and white. The full color images can be found in the on-line version, at doi:10.1016/j.actbio.2014.12.020.

### References

- Weinstein RA, Darouiche RO. Device-associated infections: a macroproblem that starts with microadherence. *Clin Infect Dis* 2001;33:1567–72.
- Campoccia D, Montanaro L, Arciola CR. The significance of infection related to orthopedic devices and issues of antibiotic resistance. *Biomaterials* 2006;27:2331–9.
- Arciola CR, Campoccia D, Speziale P, Montanaro L, Costerton JW. Biofilm formation in *Staphylococcus* implant infections. a review of molecular mechanisms and implications for biofilm-resistant materials. *Biomaterials* 2012;33:5967–82.
- Costerton JW, Stewart PS, Greenberg EP. Bacterial biofilms: a common cause of persistent infections. *Science* 1999;284:1318–22.
- Donlan RM. Biofilm formation: a clinically relevant microbiological process. *Clin Infect Dis* 2001;33:1387–92.
- Costerton JW, Montanaro L, Arciola CR. Biofilm in implant infections: its production and regulation. *Int J Artif Organs* 2005;28:1062–8.
- Campoccia D, Montanaro L, Arciola CR. A review of the biomaterials technologies for infection-resistant surfaces. *Biomaterials* 2013;34:8533–54.
- Goodman SB, Yao Z, Keeney M, Yang F. The future of biologic coatings for orthopaedic implants. *Biomaterials* 2013;34:3174–83.
- Banerjee I, Pangule R, Kane R. Antifouling coatings: recent developments in the design of surfaces that prevent fouling by proteins, bacteria, and marine organisms. *Adv Mater (Deerfield Beach, Fla)* 2011;23:690–718.
- Zhao L, Chu PK, Zhang Y, Wu Z. Antibacterial coatings on titanium implants. *J Biomed Mater Res B Appl Biomater* 2009;91B:470–80.
- Knetsch MLW, Koole LH. New strategies in the development of antimicrobial coatings: the example of increasing usage of silver and silver nanoparticles. *Polymers* 2011;3:340–66.
- Costa Fo, Carvalho IF, Montelaro RC, Gomes P, Martins MCL. Covalent immobilization of antimicrobial peptides (AMPs) onto biomaterial surfaces. *Acta Biomater* 2011;7:1431–40.
- Ulman A. Formation and structure of self-assembled monolayers. *Chem Rev* 1996;96:1533–54.
- Love JC, Estroff LA, Kriebel JK, Nuzzo RG, Whitesides GM. Self-assembled monolayers of thiolates on metals as a form of nanotechnology. *Chem Rev* 2005;105:1103–70.
- Onclin S, Ravoo BJ, Reinhoudt DN. Engineering silicon oxide surfaces using self-assembled monolayers. *Angew Chem Int Ed* 2005;44:6282–304.
- Mutin PH, Guerrero G, Vioux A. Hybrid materials from organophosphorus coupling molecules. *J Mater Chem* 2005;15:3761–8.
- Wiencek KM, Fletcher M. Bacterial adhesion to hydroxyl- and methyl-terminated alkanethiol self-assembled monolayers. *J Bacteriol* 1995;177:1959–66.
- Ostuni E et al. Self-assembled monolayers that resist the adsorption of proteins and the adhesion of bacterial and mammalian cells. *Langmuir* 2001;17:6336–43.
- Tegoulia VA, Rao W, Kalambar AT, Rabolt JF, Cooper SL. Surface properties, fibrinogen adsorption, and cellular interactions of a novel phosphorylcholine-containing self-assembled monolayer on gold. *Langmuir* 2001;17:4396–404.
- Cheng G, Zhang Z, Chen S, Bryers JD, Jiang S. Inhibition of bacterial adhesion and biofilm formation on zwitterionic surfaces. *Biomaterials* 2007;28:4192–9.
- Ploux L, Beckendorff S, Nardin M, Neunlist S. Quantitative and morphological analysis of biofilm formation on self-assembled monolayers. *Colloids Surf, B* 2007;57:174–81.
- Liu Y, Strauss J, Camesano TA. Adhesion forces between *Staphylococcus epidermidis* and surfaces bearing self-assembled monolayers in the presence of model proteins. *Biomaterials* 2008;29:4374–82.
- Bandyopadhyay D, Prashar D, Luk Y-Y. Anti-fouling chemistry of chiral monolayers: enhancing biofilm resistance on racemic surface. *Langmuir* 2011;27:6124–31.
- Hou S, Burton EA, Simon KA, Blodgett D, Luk Y-Y, Ren D. Inhibition of *Escherichia coli* biofilm formation by self-assembled monolayers of functional alkanethiols on gold. *Appl Environ Microbiol* 2007;73:4300–7.
- Kuegler R, Bouloussa O, Rondelez F. Evidence of a charge-density threshold for optimum efficiency of biocidal cationic surfaces. *Microbiology (Reading, UK)* 2005;151:1341–8.
- Thebault P, Taffin dGE, Levy R, Vandenberghe Y, Guittard F, Geribaldi S. Contact-active microbicidal gold surfaces using immobilization of quaternary ammonium thiol derivatives. *Eur J Med Chem* 2009;44:4227–34.
- Amalric J, Mutin PH, Guerrero G, Ponche A, Sotto A, Lavigne J-P. Phosphonate monolayers functionalized by silver thiolate species as antibacterial nanocoatings on titanium and stainless steel. *J Mater Chem* 2009;19:141–9.
- Torres N et al. Stability of antibacterial self-assembled monolayers on hydroxyapatite. *Acta Biomater* 2010;6:3242–55.
- Pallavicini P et al. Coordination chemistry for antibacterial materials: a monolayer of a Cu<sup>2+</sup> 2,2'-bipyridine complex grafted on a glass surface. *Dalton Trans* 2013;42:4552–60.
- Antoci V et al. The inhibition of *Staphylococcus epidermidis* biofilm formation by vancomycin-modified titanium alloy and implications for the treatment of periprosthetic infection. *Biomaterials* 2008;29:4684–90.
- Humbolt V et al. The antibacterial activity of Magainin I immobilized onto mixed thiols self-assembled monolayers. *Biomaterials* 2009;30:3503–12.
- Yliniemi K et al. The formation and characterization of ultra-thin films containing Ag nanoparticles. *J Mater Chem* 2008;18:199–206.
- Pallavicini P et al. Self-assembled monolayers of silver nanoparticles firmly grafted on glass surfaces: low Ag<sup>+</sup> release for an efficient antibacterial activity. *J Colloid Interface Sci* 2010;350:110–6.
- Kim JS et al. Antimicrobial effects of silver nanoparticles. *Nanomed Nanotechnol Biol Med* 2007;3:95–101.
- Chernousova S, Epple M. Silver as antibacterial agent: ion, nanoparticle, and metal. *Angew Chem Int Ed* 2013;52:1636–53.
- Greulich C et al. The toxic effect of silver ions and silver nanoparticles towards bacteria and human cells occurs in the same concentration range. *RSC Adv* 2012;2:6981–7.
- Agarwal A et al. Surfaces modified with nanometer-thick silver-impregnated polymeric films that kill bacteria but support growth of mammalian cells. *Biomaterials* 2010;31:680–90.
- Mei S et al. Antibacterial effects and biocompatibility of titanium surfaces with graded silver incorporation in titania nanotubes. *Biomaterials* 2014;35:4255–65.
- Tsai M-Y, Lin J-C. Surface characterization and platelet adhesion studies of self-assembled monolayer with phosphonate ester and phosphonic acid functionalities. *J Biomed Mater Res* 2001;55:554–65.
- Bouffé C, Bony C, Courties G, Jørgensen C, Noel D. IL-6-dependent PGE<sub>2</sub> secretion by mesenchymal stem cells inhibits local inflammation in experimental arthritis. *PLoS ONE* 2010;5:e14247.
- Djouad F et al. Reversal of the immunosuppressive properties of mesenchymal stem cells by tumor necrosis factor  $\alpha$  in collagen-induced arthritis. *Arthritis Rheum* 2005;52:1595–603.

- [42] Balazs DJ et al. Inhibition of bacterial adhesion on PVC endotracheal tubes by RF-oxygen glow discharge, sodium hydroxide and silver nitrate treatments. *Biomaterials* 2004;25:2139–51.
- [43] Mendes GCC, Brandão TRS, Silva CLM. Ethylene oxide sterilization of medical devices: a review. *Am J Infect Control* 2007;35:574–81.
- [44] Schoenfisch MH, Pemberton JE. Air stability of alkanethiol self-assembled monolayers on silver and gold surfaces. *J Am Chem Soc* 1998;120:4502–13.
- [45] Willey TM, Vance AL, van Buuren T, Bostedt C, Terminello LJ, Fadley CS. Rapid degradation of alkanethiol-based self-assembled monolayers on gold in ambient laboratory conditions. *Surf Sci* 2005;576:188–96.
- [46] Bensebaa F, Zhou Y, Deslandes Y, Kruus E, Ellis TH. XPS study of metal–sulfur bonds in metal–alkanethiolate materials. *Surf Sci* 1998;405:L472–6.
- [47] Esplandiu MJ, Noeske PLM. XPS investigations on the interactions of 1,6-hexanedithiol/Au(111) layers with metallic and ionic silver species. *Appl Surf Sci* 2002;199:166–82.
- [48] Sudo H, Kodama HA, Amagai Y, Yamamoto S, Kasai S. In vitro differentiation and calcification in a new clonal osteogenic cell line derived from newborn mouse calvaria. *J Cell Biol* 1983;96:191–8.
- [49] Quarles LD, Yohay DA, Lever LW, Caton R, Wenstrup RJ. Distinct proliferative and differentiated stages of murine MC3T3-E1 cells in culture: an in vitro model of osteoblast development. *J Bone Miner Res* 1992;7:683–92.
- [50] Akiyama T et al. Silver oxide-containing hydroxyapatite coating has in vivo antibacterial activity in the rat tibia. *J Orthop Res* 2013;31:1195–200.
- [51] Gosheger G et al. Silver-coated megaendoprostheses in a rabbit model—an analysis of the infection rate and toxicological side effects. *Biomaterials* 2004;25:5547–56.
- [52] Honda M et al. In vitro and in vivo antimicrobial properties of silver-containing hydroxyapatite prepared via ultrasonic spray pyrolysis route. *Mater Sci Eng, C* 2013;33:5008–18.
- [53] Liu Y et al. The antimicrobial and osteoinductive properties of silver nanoparticle/poly (D,L-lactic-co-glycolic acid)-coated stainless steel. *Biomaterials* 2012;33:8745–56.
- [54] Shimazaki T et al. In vivo antibacterial and silver-releasing properties of novel thermal sprayed silver-containing hydroxyapatite coating. *J Biomed Mater Res B Appl Biomater* 2010;92B:386–9.
- [55] Zhao L et al. Antibacterial nano-structured titania coating incorporated with silver nanoparticles. *Biomaterials* 2011;32:5706–16.
- [56] De Giglio E et al. An innovative, easily fabricated, silver nanoparticle-based titanium implant coating: development and analytical characterization. *Anal Bioanal Chem* 2013;405:805–16.
- [57] Ewald A, Gluckermann SK, Thull R, Gbureck U. Antimicrobial titanium/silver PVD coatings on titanium. *Biomed Eng Online* 2006;5:22.
- [58] Necula BS, van LJP, Fratila-Apachitei LE, Zaat SAJ, Apachitei I, Duszczczyk J. In vitro cytotoxicity evaluation of porous TiO<sub>2</sub>-Ag antibacterial coatings for human fetal osteoblasts. *Acta Biomater* 2012;8:4191–7.
- [59] Bai X, Sandukas S, Appleford M, Ong JL, Rabiei A. Antibacterial effect and cytotoxicity of Ag-doped functionally graded hydroxyapatite coatings. *J Biomed Mater Res B Appl Biomater* 2012;100B:553–61.
- [60] Lee JS, Murphy WL. Functionalizing calcium phosphate biomaterials with antibacterial silver particles. *Adv Mater (Weinheim, Ger)* 2013;25:1173–9.
- [61] Helmy R, Fadeev AY. Self-assembled monolayers supported on TiO<sub>2</sub>: comparison of C18H37SiX3 (X = H, Cl, OCH3), C18H37Si(CH3)2Cl, and C18H37PO(OH)2. *Langmuir* 2002;18:8924–8.
- [62] Marcinko S, Fadeev AY. Hydrolytic stability of organic monolayers supported on TiO<sub>2</sub> and ZrO<sub>2</sub>. *Langmuir* 2004;20:2270–3.
- [63] Mani G et al. Stability of self-assembled monolayers on titanium and gold. *Langmuir* 2008;24:6774–84.
- [64] Gristina A. Biomaterial-centered infection: microbial adhesion versus tissue integration. *Science* 1987;237:1588–95.
- [65] Marsich E et al. Biological responses of silver-coated thermosets: an in vitro and in vivo study. *Acta Biomater* 2013;9:5088–99.